



Crack propagation in a material with random toughness

L. CHEN¹, R. BALLARINI¹ and M. GRIGORIU²

¹*Department of Civil Engineering, Case Western Reserve University, Cleveland, Ohio 44106-7201, U.S.A.*

²*Department of Civil Engineering, Cornell University, Ithaca, NY 14853, U.S.A.*

Received 11 July 2003; accepted in revised form 25 November 2003

Abstract. An efficient Monte Carlo procedure is presented for characterizing the propagation of a crack in a material whose fracture toughness is a random field. The simulations rely on accurate approximate solutions of the integral equations that govern the dislocation densities, stress intensity factors, and energy release rates of curvilinear cracks. For a plate containing an edge crack that propagates towards a subsurface crack representing a traction-free boundary, results for the distributions of crack trajectories, critical applied far-field stresses, and nominal fracture toughness are presented for various parameters that quantify the randomness of the material's critical energy release rate. A demonstrative probabilistic model for crack trajectories is built and size effects are discussed.

Key words: Crack trajectories, Monte Carlo simulation, random toughness, size effects, stochastic fracture mechanics.

1. Introduction

Heterogeneous quasi-brittle materials are associated with spatially varying strength and fracture toughness parameters that result in tortuous crack trajectories and size-dependent nominal fracture toughness exhibiting significant statistical scatter. Attempts to model these phenomena include the statistical fracture mechanics (SFM) procedures developed by Kunin (1994), Chudnovsky and Gorelik (1996), Chudnovsky et al. (1997), Kunin and Dearth (1998), Arwade (1999) and Chen (2000). These models characterize, through various approximations, cracking along curved trajectories in materials with random critical energy release rate, 2γ . The approach proposed by Kunin (1994), Chudnovsky et al. (1997) and Kunin and Dearth (1998) is based on the concept of averaging over an ensemble of macroscopically identical fracture specimens, or equivalently, associating with a single specimen an ensemble Ω of virtual crack trajectories and expressing the average in the form of a functional integral over Ω . By adopting relatively crude approximations of the stress intensity factors, K_I , K_{II} and energy release rate, G , of a curvilinear crack, the functional integration is reduced to solving a diffusion-type partial differential equation, to which well-developed techniques are applied for averaging over sets of Brownian paths.

To eliminate the need of performing functional integration, Monte Carlo simulation of crack trajectories has been proposed by Chudnovsky and Gorelik (1996), Arwade (1999) and Chen (2000). In Chudnovsky and Gorelik's semi-empirical procedure, experimentally observed crack trajectories are first described as smoothed Brownian paths, and 2γ along these paths is assumed to be a random variable. For each realization, the finite element method is used to calculate K_I , K_{II} , and $G = (K_I^2 + K_{II}^2)/E$ (E is Young's modulus) of the propagating crack, which is assumed to propagate according to the Griffith criterion, $G = 2\gamma$. Relev-

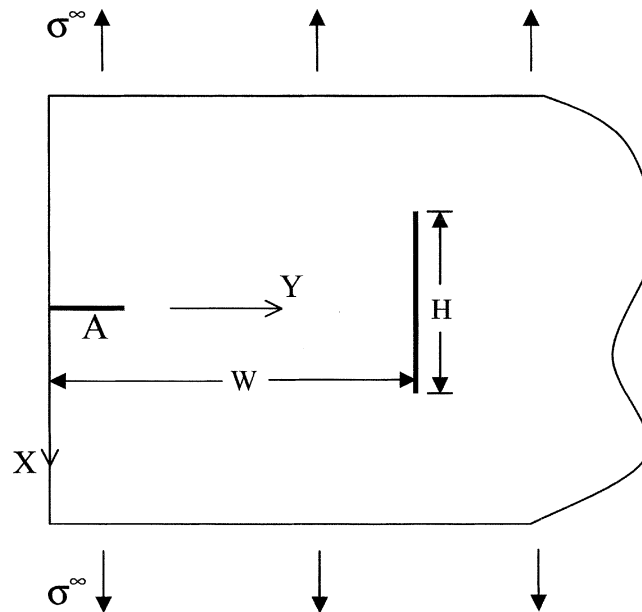


Figure 1. A semi-infinite plate with an edge crack and an inner crack.

ant statistics of the process are evaluated, including the dependence of the nominal fracture toughness on specimen size.

Arwade performed similar computations for intergranular cracking in polycrystalline aluminum plates. In his model the randomness of the trajectories results from the geometry of the microstructure (or more specifically of the grain boundaries), which is approximated as a Poisson–Voronoi tessellation. The main conclusion of Arwade’s calculations is that crack trajectories in such a material correspond to a scaled Brownian motion. Chudnovsky and Gorelik’s and Arwade’s models both rely on the finite element method to calculate crack-tip parameters; within the context of Monte Carlo simulation this procedure, which involves remeshing after each increment of crack growth, is time consuming and cumbersome. To reduce the complexity of remeshing, Chudnovsky and Gorelik’s finite element models replace the crack trajectory with two straight line segments that retain the tangent angle of the trajectory at the crack tip. This procedure was introduced by Chudnovsky and Gorelik and Brandinelli and Ballarini (2000) because it was demonstrated by Rubinstein (1990) that crack-tip parameters are sensitive not to the details of a cracks trajectory’s shape, but only to its shape near the tip. This paper presents an efficient integral equation-based Monte Carlo simulation procedure for characterizing the propagation of cracks in materials with random toughness. Because the singular integral equation represents the canonical form of a crack stress analysis, the procedure is the most efficient method for Monte Carlo simulation of cracks propagating in materials with random 2γ . The model is demonstrated through calculations of an edge crack propagating through a material whose 2γ takes independent identically distributed values at different points.

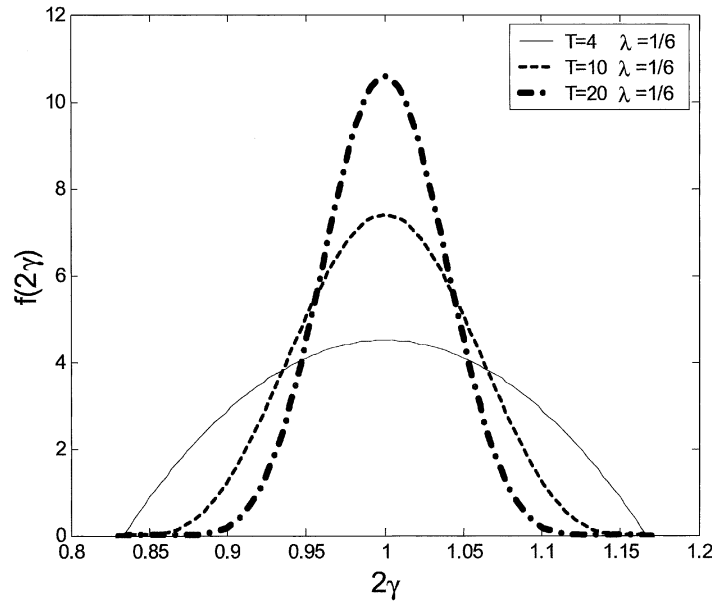


Figure 2. Beta distribution.

2. Formulation

Figure 1 is a schematic of the physical problem. A semi-infinite plate containing an edge crack of length A and a subsurface crack of length H is loaded by a uniform far-field stress σ^∞ . The subsurface crack is introduced as an additional traction-free surface to capture size-dependent fracture behavior. As discussed in the previous section, the stress intensity factors and energy release rate produced by the far-field loading are K_I , K_{II} , and G , respectively, and the critical energy release rate, 2γ , is assumed to take independent identically distributed values according to a prescribed distribution. The illustrative results presented in this paper correspond to the truncated Beta-distribution defined by

$$f(2\gamma) = \Gamma(T)[(2\gamma - 1 + \lambda)]^{T/2-1} / \Gamma^2\left(\frac{T}{2}\right) (2\lambda)^{T-1}. \tag{1}$$

As shown in Figure 2, parameters T and λ quantify, respectively, the tightness and the range of the distribution. It is assumed that crack extension obeys the Griffith criterion, $G = 2\gamma$, along a path that maximizes the energy released. Consider a crack tip that has reached point i , as shown in Figure 3, whose stress intensity factors and energy release rate are K_{I_i} , K_{II_i} and G_i , respectively. The subsequent crack tip location, $i + 1$, is assumed to be always ahead of point i (the crack must advance), and is reached by a straight constant length extension, r_o , determined using the following procedure (r_o is some characteristic length of the material's microstructure, and will henceforth be referred to as the grain size). The direction of propagation, which is defined by θ_i ($\theta_i \in [0, \pi]$), is determined by comparing the energy release rate along all possible directions (a constant increment equal to 0.5° is used in the calculations), G_{θ_i} , with the critical energy release rate along these directions, $2\gamma_{\theta_i}$, prescribed through the Beta distribution. Crack propagation can be either stable (Griffith equilibrium is maintained with an increasing load), or unstable (Griffith equilibrium is maintained with a decreasing

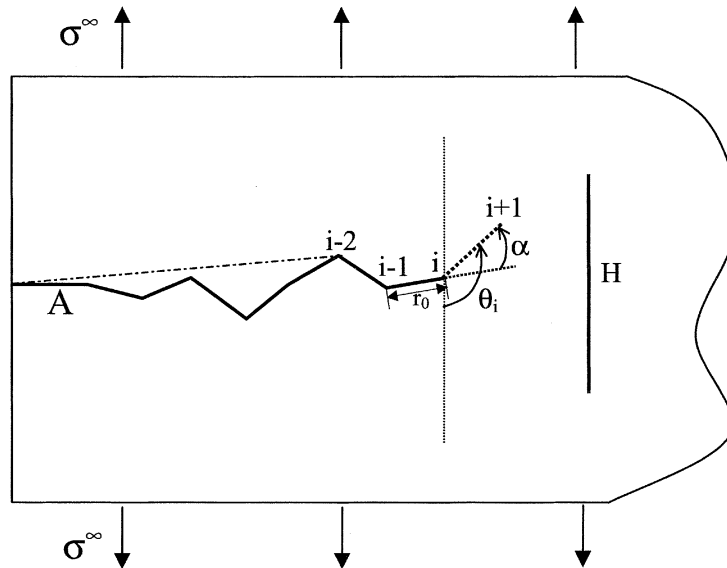


Figure 3. An edge crack propagating along a random path, and the associated three-segment approximation of the crack profile.

load). The decision tree associated with determination of direction and equilibrium load is as follows.

Two possibilities exist. In the first $G_{\theta_i} < 2\gamma_{\theta_i}$ for all θ_i . For this situation an increase in load is applied to extend the crack, along the direction that maximizes $G_{\theta_i}/2\gamma_{\theta_i}$. The second case corresponds to $G_{\theta_i} > 2\gamma_{\theta_i}$ for one or more θ_i . For this case equilibrium is maintained during the extension by decreasing the load, and the direction chosen maximizes $G_{\theta_i} - 2\gamma_{\theta_i}$.

The computational difficulties that arise in Monte Carlo simulations involving large numbers of realizations and parameters that describe the random distribution of critical energy release rate, include calculation of K_{I_i} , K_{II_i} and G_i . The following procedure is introduced that offers promise in such studies.

The crack stress analysis is formulated using the method of distributed dislocations. As shown in Figure 4, for a discrete dislocation at points $z_0 = X + iY$ in a half-plane, define $b = \mu([u_r] + i[v_\theta])e^{i\theta_d}/\pi i(\kappa + 1)$, where θ_d indicates the angle between the tangent to the crack trajectory at point z_0 and the X-axis, $[u_r]$ and $[v_\theta]$ represent the magnitudes of the (polar) displacement discontinuities across the slip plane, μ is the shear modulus, ν is Poisson's ratio, $\kappa = 3-4\nu$ for plane strain, and $\kappa = (3 - \nu)/(1 + \nu)$ for plane stress. The stress components produced by the dislocation at any point $z = X + iY$ include

$$\sigma_{\theta\theta} + i\sigma_{r\theta} = b \left\{ \frac{1}{z - z_0} - \frac{1}{z - \bar{z}_0} + \frac{z_0 - \bar{z}_0}{(\bar{z} - z_0)^2} + e^{2i\theta_\sigma} \left[\frac{\bar{z} - \bar{z}_0}{(z - \bar{z}_0)^2} + \frac{\bar{z}_0 - \bar{z}}{(z - z_0)^2} \right] \right\} + \bar{b} \left\{ \frac{1}{\bar{z} - \bar{z}_0} - \frac{1}{\bar{z} - z_0} + \frac{\bar{z}_0 - z_0}{(z - \bar{z}_0)^2} + e^{2i\theta_\sigma} \left[\frac{1}{z - z_0} + \frac{z_0 - z}{(z - \bar{z}_0)^2} + \frac{2(\bar{z} - z)(z_0 - \bar{z}_0)}{(z - \bar{z}_0)^3} \right] \right\}, \tag{2}$$

where θ_σ represents the angle between the tangent to the crack trajectory at point z and the X-axis. Next define the dislocations density $\beta(z_0)$ as

$$\beta(z_0) = \frac{\partial b}{\partial z_0} = \frac{\mu}{\pi i(\kappa + 1)} \frac{\partial}{\partial z_0} [(u_r) + i(v_\theta)]e^{i\theta_d}.$$

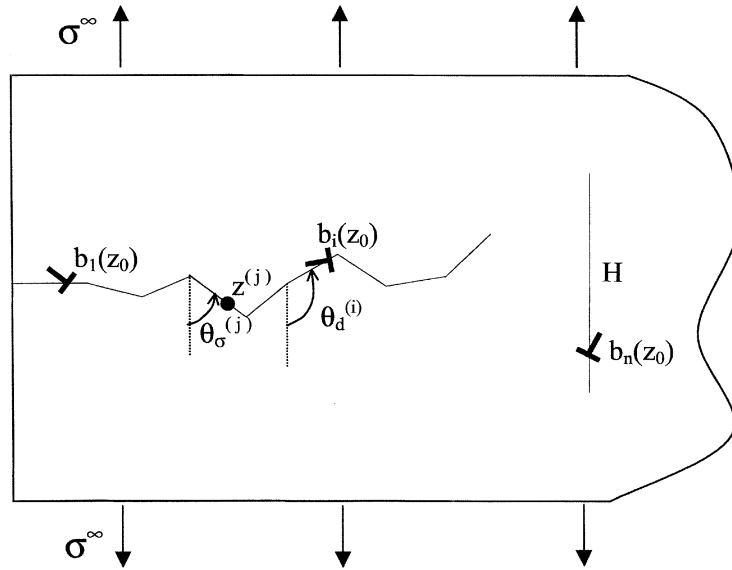


Figure 4. Illustration of dislocation points along a crack.

The subsurface crack, together with the $n - 1$ linear segments that comprise the crack trajectory, are represented by n unknown dislocation densities, $\beta_1(z_0), \beta_2(z_0) \dots \beta_n(z_0)$. This enables the zero-traction boundary conditions along these surfaces to be written as n coupled singular integral equations of the form

$$\begin{aligned}
 & \int \hat{\beta}_1(z_0^{(1)})k_1(z^{(1)}, z_0^{(1)}) dz_0^{(1)} + \int \overline{\hat{\beta}_1(z_0^{(1)})}k_2(z^{(1)}, z_0^{(1)}) \overline{dz_0^{(1)}} \\
 & + \int \hat{\beta}_2(z_0^{(2)})k_1(z^{(1)}, z_0^{(2)}) dz_0^{(2)} + \int \overline{\hat{\beta}_2(z_0^{(2)})}k_2(z^{(1)}, z_0^{(2)}) \overline{dz_0^{(2)}} \\
 & + \dots \\
 & + \int \hat{\beta}_n(z_0^{(n)})k_1(z^{(1)}, z_0^{(n)}) dz_0^{(n)} + \int \overline{\hat{\beta}_n(z_0^{(n)})}k_2(z^{(1)}, z_0^{(n)}) \overline{dz_0^{(n)}} = -\sin^2 \theta_\sigma^{(1)} + i \sin \theta_\sigma^{(1)} \cos \theta_\sigma^{(1)} \\
 & + \int \hat{\beta}_1(z_0^{(1)})k_1(z^{(i)}, z_0^{(1)}) dz_0^{(1)} + \int \overline{\hat{\beta}_1(z_0^{(1)})}k_2(z^{(i)}, z_0^{(1)}) \overline{dz_0^{(1)}} \\
 & + \int \hat{\beta}_2(z_0^{(2)})k_1(z^{(i)}, z_0^{(2)}) dz_0^{(2)} + \int \overline{\hat{\beta}_2(z_0^{(2)})}k_2(z^{(i)}, z_0^{(2)}) \overline{dz_0^{(2)}} \\
 & + \dots \\
 & + \int \hat{\beta}_n(z_0^{(n)})k_1(z^{(i)}, z_0^{(n)}) dz_0^{(n)} + \int \overline{\hat{\beta}_n(z_0^{(n)})}k_2(z^{(i)}, z_0^{(n)}) \overline{dz_0^{(n)}} = -\sin^2 \theta_\sigma^{(i)} + i \sin \theta_\sigma^{(i)} \cos \theta_\sigma^{(i)} \\
 & + \dots
 \end{aligned}$$

Table 1. Comparison of 3-seg approximation method and N-segment method, $\theta = 15^\circ$

W	H	N-seg KI	3-seg KI	Error (%)	N-seg KII	3-seg KII	Error (%)
7.2	7.5	0.705514	0.711935	0.91	0.189538	0.186986	1.35
7.5	7.5	0.696560	0.701603	0.72	0.168043	0.166507	0.91
8.0	7.5	0.698604	0.702427	0.55	0.156930	0.156151	0.50
10.0	7.5	0.679966	0.682331	0.35	0.161389	0.161201	0.12
14.0	7.5	0.644033	0.645737	0.26	0.178234	0.178159	0.04
20.0	7.5	0.630640	0.632138	0.24	0.181920	0.181864	0.03

$$\begin{aligned}
 & + \int \hat{\beta}_1(z_0^{(1)})k_1(z^{(n-1)}, z_0^{(1)}) dz_0^{(1)} + \int \overline{\hat{\beta}_1(z_0^{(1)})}k_2(z^{(n-1)}, z_0^{(1)}) \overline{dz_0^{(1)}} \\
 & + \int \hat{\beta}_2(z_0^{(2)})k_1(z^{(n-1)}, z_0^{(2)}) dz_0^{(2)} + \int \overline{\hat{\beta}_2(z_0^{(2)})}k_2(z^{(n-1)}, z_0^{(2)}) \overline{dz_0^{(2)}} \\
 & + \dots \\
 & + \int \hat{\beta}_n(z_0^{(n)})k_1(z^{(i)}, z_0^{(n)}) dz_0^{(n)} + \int \overline{\hat{\beta}_n(z_0^{(n)})}k_2(z^{(n-1)}, z_0^{(n)}) \overline{dz_0^{(n)}} = -\sin^2 \theta_\sigma^{(n-1)} \\
 & + i \sin \theta_\sigma^{(n-1)} \cos \theta_\sigma^{(n-1)} + \int \hat{\beta}_1(z_0^{(1)})k_1(z^{(n)}, z_0^{(1)}) dz_0^{(1)} + \int \overline{\hat{\beta}_1(z_0^{(1)})}k_2(z^{(n)}, z_0^{(1)}) \overline{dz_0^{(1)}} \\
 & + \int \hat{\beta}_2(z_0^{(2)})k_1(z^{(n)}, z_0^{(2)}) dz_0^{(2)} + \int \overline{\hat{\beta}_2(z_0^{(2)})}k_2(z^{(n)}, z_0^{(2)}) \overline{dz_0^{(2)}} \\
 & + \dots \\
 & + \int \hat{\beta}_n(z_0^{(n)})k_1(z^{(n)}, z_0^{(n)}) dz_0^{(n)} + \int \overline{\hat{\beta}_n(z_0^{(n)})}k_2(z^{(n)}, z_0^{(n)}) \overline{dz_0^{(n)}} = 0.
 \end{aligned} \tag{3}$$

The right-hand sides of the equations represent the traction produced along the lines that define the subsurface crack and the tortuous crack, and the kernels $k_1(z, z_0)$ and $k_2(z, z_0)$ represent the two functions within the brackets in Equation (2). In principle, the singular integral equations can be reduced to a system of algebraic equations using the Erdogan–Gupta method (Erdogan et al., 1973), which relies on certain properties of Chebyshev polynomials. However, for a meandering crack trajectory comprised of a large number of segments this method is not feasible; accurate stress intensity factors require the solution of unacceptably large systems of algebraic equations. Brandinelli and Ballarini (2000) suggested that in Monte Carlo simulations it suffices to approximate the extended edge crack profile using three segments, and to apply the Erdogan–Gupta procedure to this approximate crack trajectory. As shown in Figure 3, the approximate trajectory shown by dashed lines connects the initial point and point $i - 2$. Thus for the problem at hand the crack stress analysis is reduced from n integral equations to four; three along the approximate trajectory, and one along the subsurface crack.

The accuracy of the approximation was demonstrated by Brandinelli and Ballarini (2000) through specific examples. To check whether this approximation is sufficient for calculating the crack-tip parameters of a meandering crack interacting with a subsurface crack, the stress

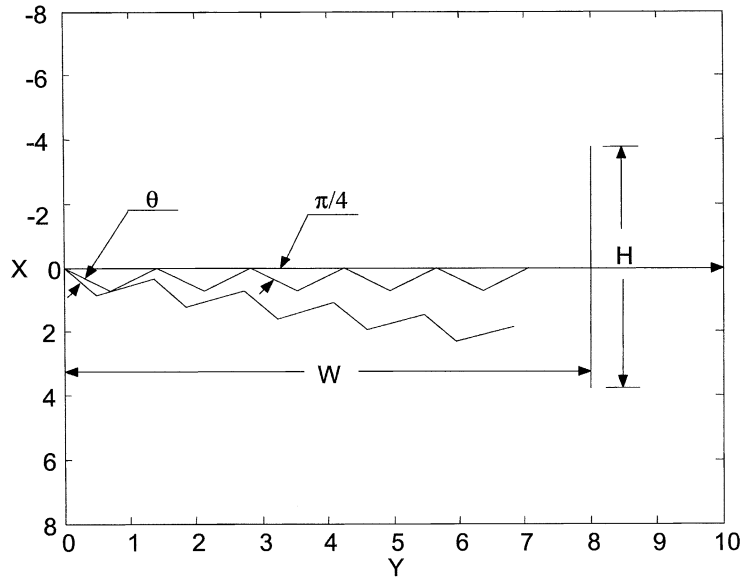


Figure 5. Configuration for the testing of 3-segment approximation method.

intensity factors of the ten segment crack configurations shown in Figure 5 are calculated and compared to those of the three-segment approximation. In the first, the zig-zag crack trajectory is, on the average, perpendicular to the free surfaces, while in the second it is on the average rotated through an angle $\theta - \pi/4$ with respect to the free surfaces. Table 1 shows that the maximum errors of the three-segment approximation method for $\theta = 15^\circ$ are less than 2%.

These results, together with those presented by Brandinelli and Ballarini, provide confidence that numerical solution of the three segment approximate crack trajectories provide sufficiently accurate stress intensity factors of a meandering crack. As shown in Figure 3, to determine the direction α of the extension of the crack that has reached point i , knowledge is required of the stress intensity factors and energy release rate for an arbitrary extension θ_i . Rather than calculating these parameters for all possible extensions using the integral equation method, use is made of the following formulas derived by Cotterell and Rice (1980) for infinitesimally short kinks

$$K_I(\alpha) = \frac{1}{4} \left(3 \cos \frac{\alpha}{2} + \cos \frac{3\alpha}{2} \right) K_{I_i} - \frac{3}{4} \left(\sin \frac{\alpha}{2} + \sin \frac{3\alpha}{2} \right) K_{II_i}, \tag{4}$$

$$K_{II}(\alpha) = \frac{1}{4} \left(\sin \frac{\alpha}{2} + \sin \frac{3\alpha}{2} \right) K_{I_i} + \frac{1}{4} \left(\cos \frac{\alpha}{2} + 3 \cos \frac{3\alpha}{2} \right) K_{II_i}, \tag{5}$$

so that the energy release rate for a finite extension r_o is approximated as

$$G_{\theta_i} = \frac{K_I^2(\alpha) + K_{II}^2(\alpha)}{E}. \tag{6}$$

3. Results and discussion

Based on the geometry shown in Figure 1, two cases are studied in this paper. The first corresponds to very short initial cracks, $A/W \rightarrow 0$, and the second to moderate-length cracks that

Table 2. Critical crack-tip position

	A/W=0.1		A/W=0.25		A/W=0.5	
	Steps	Position	Steps	Position	Steps	Position
$r_0 = 0.1$	23	22.3	27	52.7	52	105.2
$r_0 = 0.5$	7	23.5	7	53.5	13	106.5
$r_0 = 1.0$	2	22.0	3	53.0	6	106.0
$r_0 = 5.0$	2	30.0	2	60.0	2	110.0
$r_0 = 10.0$	2	40.0	2	70.0	2	120.0

sense the presence of the subsurface crack, $A/W \in [0.1, 0.5]$. As discussed subsequently, long cracks are associated, as a result of their interaction with the subsurface crack, with a stochastic process that is quite different than the process that drives short surface flaws. In the calculations and subsequent discussions the length parameters are normalized with respect to r_0 , i.e., $a = A/r_0$, $x = X/r_0$, $y = Y/r_0$.

Typical results of the Monte Carlo simulations for $A/W \rightarrow 0$, $r_0 = 1.0$ are presented in Figures 6–9. Recall from Equation (1) that parameter λ defines the upper and lower limit of the critical energy release rate, while T quantifies the tightness of its distribution. Figure 6 shows that as the level of randomness increases, so does the envelope that contains all possible crack profiles. The characteristics of the trajectories are quantified through their variance S^2 , whose normalized value, $s^2 = S^2/r_0^2$, is plotted in Figure 7 as a function of the distance ahead of the initial crack tip. While the results are not included here, the mean value of the crack path was found to be zero. It is observed that the variance of the crack paths increases linearly with y , suggesting that the crack trajectory process can be modeled by a scaled Brownian motion.

Figure 8 presents the normalized equilibrium stress, $\sigma_{\text{nor}}^\infty = \sigma^\infty / \sqrt{2\gamma_{\text{mean}} E / \pi A}$, as a function of crack extension for one realization. This plot illustrates that initial crack extension may not be associated with the peak applied stress. Instead, as shown in Table 2, the crack may extend by some distance before becoming unstable. The peak stress for each realization is used to calculate the critical value of the applied energy release rate, $G_{\text{max}}^\infty = [(1.12\sigma_{\text{max}}^\infty)^2 \cdot \pi \cdot A] / E$. This parameter represents the nominal fracture toughness that would be measured in a fracture mechanics experiment to assess the sensitivity of the material to cracks. Typical distributions are shown in Figure 9.

Consider next cases where the propagating crack interacts with the subsurface crack. Results are calculated for initial crack lengths A/W equal to 0.1, 0.25 and 0.5, extension lengths r_0 equal to 0.1, 0.5, 1.0, 5.0 and 10.0, and $H/W = 6$. The material toughness distribution is quantified as $T = 4$ and $\lambda = 2/3$.

Figure 10 shows that the crack trajectories for these finite sized specimens differ in character from those of the short cracks. As they grow towards the free surface, they align themselves perpendicular to the applied stress field. These trajectories demonstrate the coupling between the random toughness and the free boundary. The statistical properties of the crack trajectories are studied for $A/W = 0.1$. Let $X(y)$, $y \in [20, 200]$ denote the crack trajectory process, and let $x_i(y)$ be samples of $X(y)$. The mean and standard deviation of $X(y)$ can be estimated by

$$\mu(y) = (1/n) \sum_{i=1}^n x_i(y), \quad (7)$$

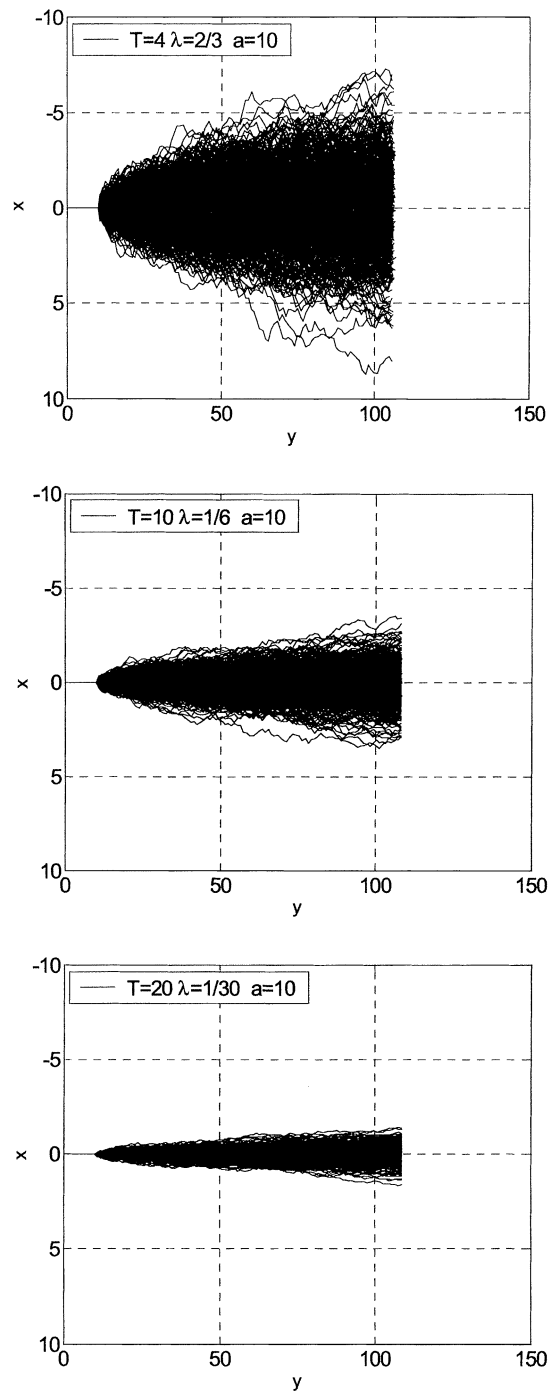


Figure 6. Typical crack trajectories for three levels of randomness of critical energy release rate.

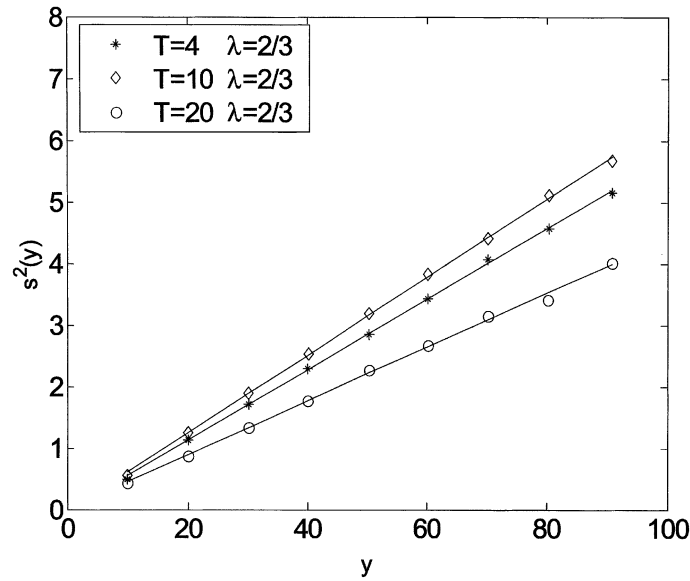


Figure 7. Estimated variance of crack trajectory process.

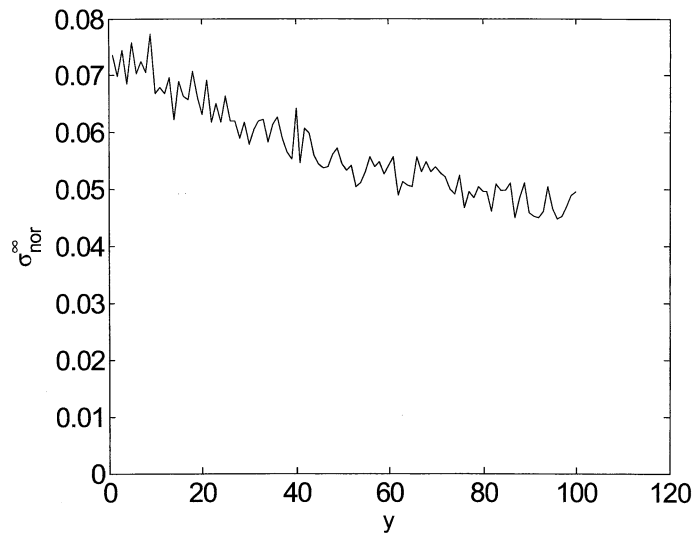


Figure 8. Typical equilibrium stress as a function of crack extension.

$$\sigma(y) = [(1/(n - 1)) \sum_{i=1}^n (x_i(y) - \mu(y))^2]^{1/2}. \tag{8}$$

Figure 11 shows $\mu(y)$ and $\sigma(y)$ for different values of r_o . As expected, $\mu(y)$ oscillates about zero. Since the standard deviation $\sigma(y)$ is not an increasing function of y , $X(y)$ is not a Brownian motion.

Figure 12 shows that kurtosis coefficients, $Kur(y)$, are close to 3 and that the skewness coefficients, $Skew(y)$, are almost equal to zero. These results suggest that the crack trajectory process $X(y)$ can be assumed to be Gaussian, i.e.,

$$X(y) = \mu(y) + \sigma(y)Z(y), \quad y \geq 0, \tag{9}$$

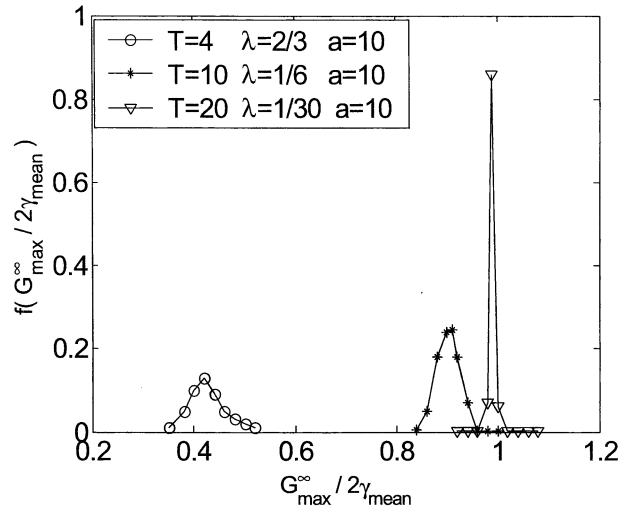


Figure 9. Distributions of critical nominal energy release rate for various levels of randomness of critical energy release rate (normalized with respect to the average of the Beta-distribution).

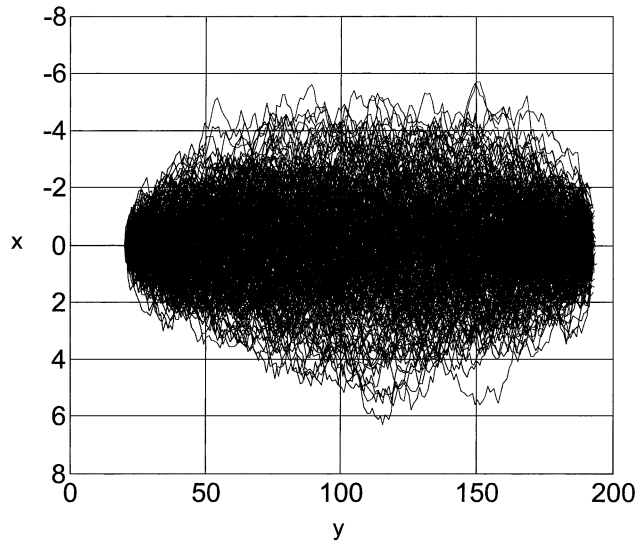


Figure 10. Typical crack trajectories, $a = 20 r_0 = 1.0$.

where $Z(y)$ is a random process such that $Z(y) \sim N(0, 1)$ for each $y \geq 0$. The skewness and kurtosis coefficients of $X(y)$ are the third and fourth central moments of $X(y)$ scaled by $\sigma(y)^3$ and $\sigma(y)^4$, respectively. Skewness and kurtosis coefficients are 0 and 3 for Gaussian variables.

The path-dependence of the crack trajectory is quantified next by considering the scaled crack trajectories

$$\hat{x}_i(y) = (x_i(y) - \mu(y))/\sigma(y). \tag{10}$$

The covariance function of the scale trajectories defined by Equation (10) can be estimated by

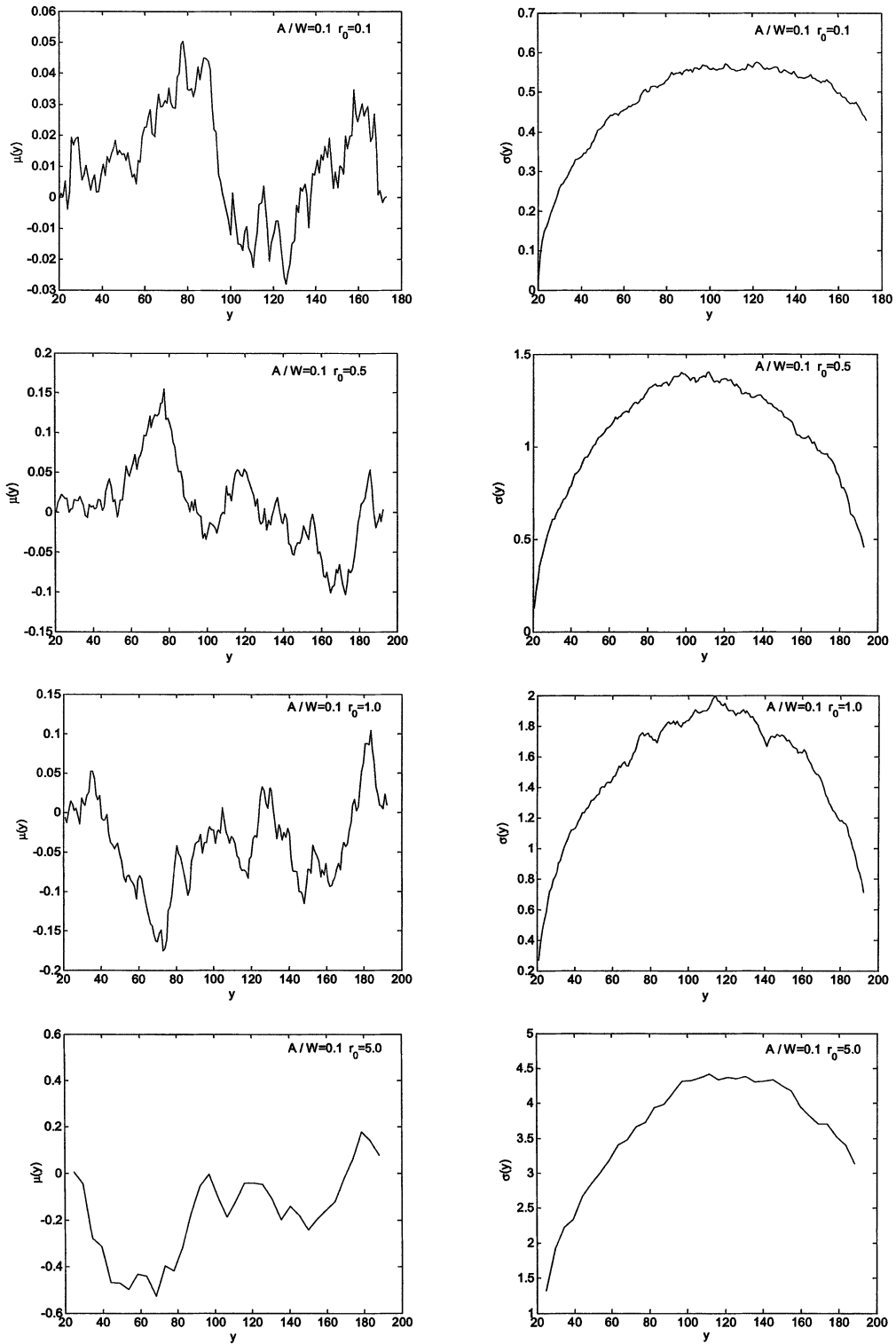


Figure 11. Expected value and standard deviation of crack trajectory process.

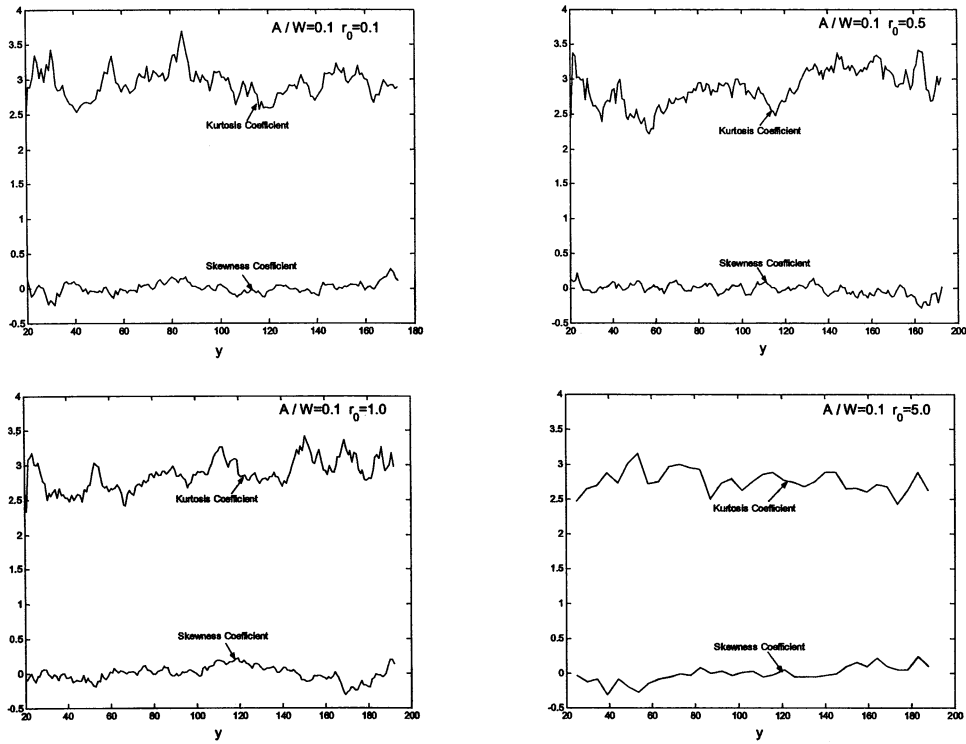


Figure 12. Kurtosis and skewness coefficients.

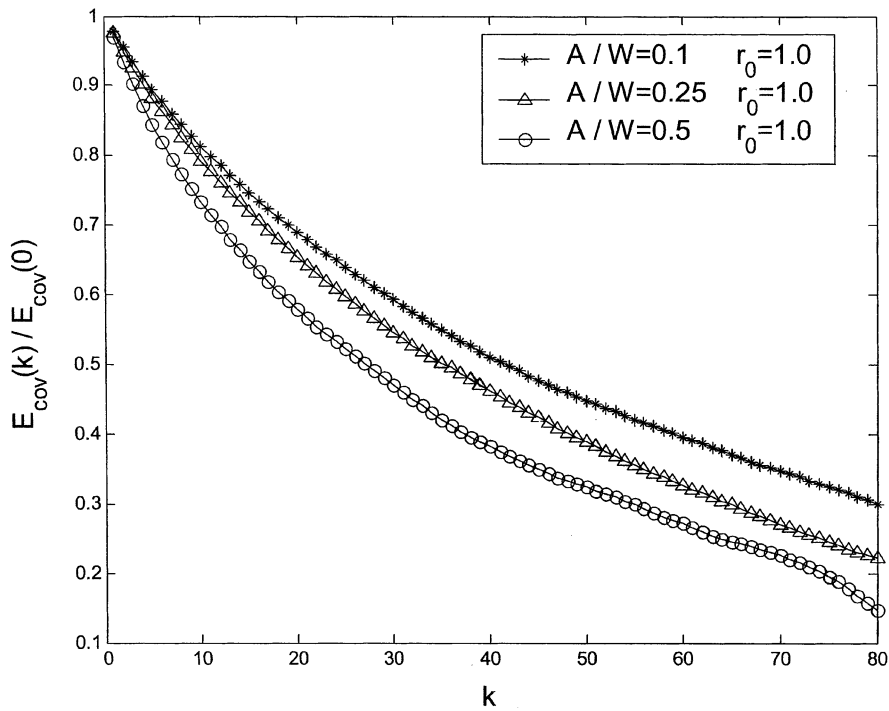


Figure 13. Estimated covariance function of crack trajectory process.

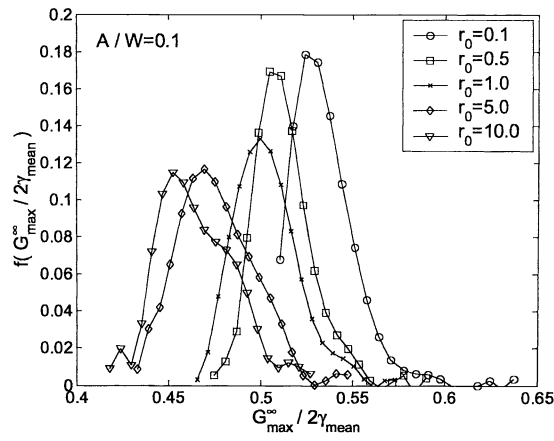


Figure 14- (a)

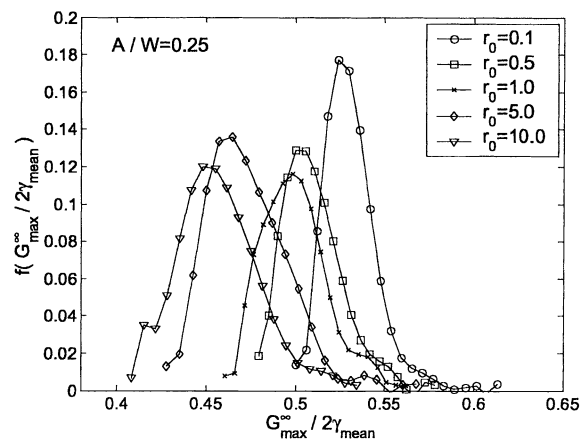


Figure 14- (b)

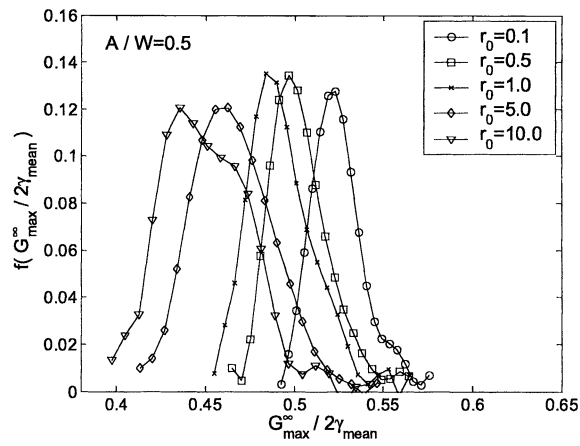


Figure 14- (c)

Figure 14. Size effects on critical energy release rate.

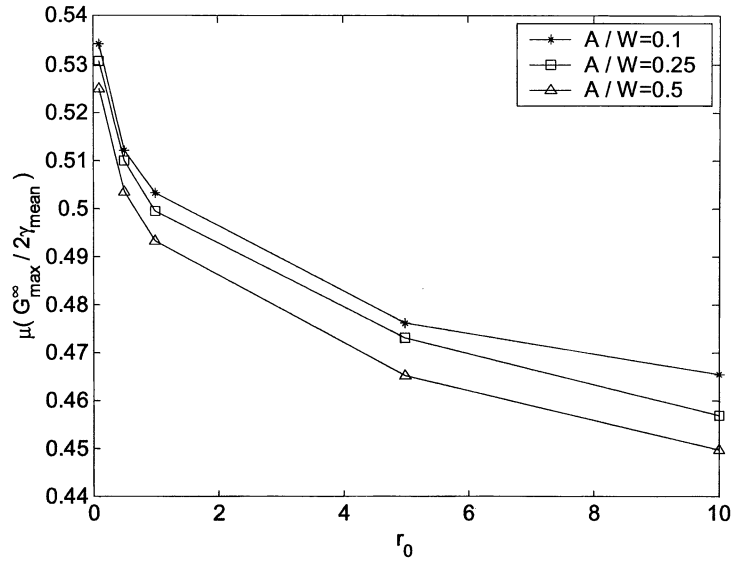


Figure 15-(a)

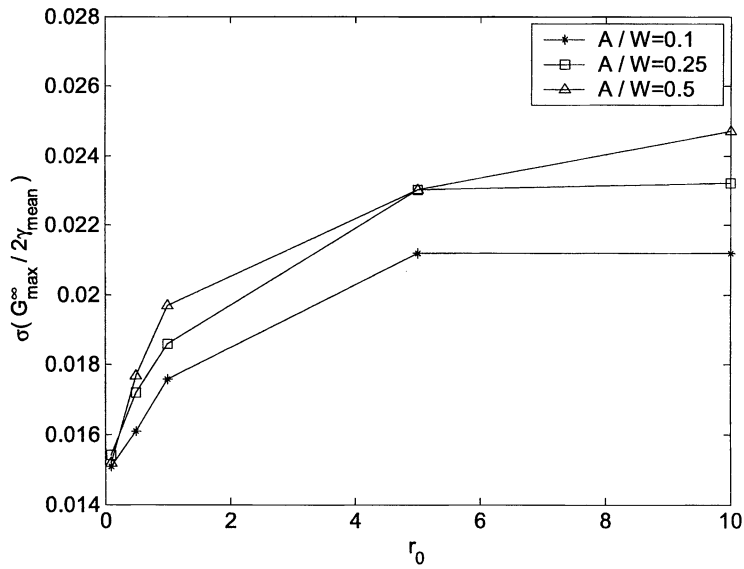


Figure 15-(b)

Figure 15. Variation of statistic parameters of the critical energy release rate.

$$E_{\text{cov}}(k) = \frac{1}{n-k} \sum_{i=1}^{n-k} \text{cov}(\hat{X}(y_i), \hat{X}(y_{i+k})), \quad k < n, \quad (11)$$

where k denotes the space lag. Figure 13 shows $E_{\text{cov}}(k)/E_{\text{cov}}(0)$ for several values of a . The slow decay of E_{cov} with k suggests that the crack trajectory process exhibits in this case long-range dependence.

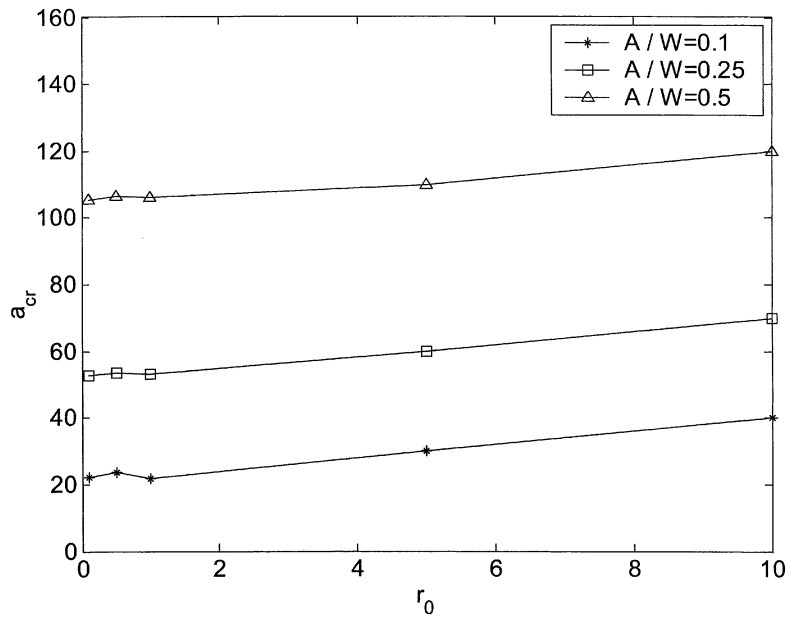


Figure 16. Variation of critical point positions.

The dependence of critical energy release rate on the size of the average grain relative to the specimen size is shown in Figures 14–16. Figure 14 shows, for various initial crack sizes, that the nominal critical energy release rate increases with decreasing grain size. This results because the number of increments during the extension, and in turn the probability that the crack tip encounters higher values of 2γ , increases with decreasing grain size. These same size effects are plotted in Figure 15 in terms of expected value and standard deviation as functions of grain size. It is observed that for the uncorrelated critical energy release rate function used in this work, the size effect is relatively weak.

The stochastic nature of the energy release rate is responsible for a certain amount of stable crack propagation. Figure 16 lists, for various initial crack lengths, the number of crack extension steps, and the position (the projected length of the crack) associated with the maximum applied far-field stress. As expected, the number of steps increases with decreasing grain size.

4. Conclusions

This paper has demonstrated that Monte Carlo simulations of crack propagation in a material with random toughness can be performed efficiently by using singular integral equations together with accurate approximations of crack profiles. This efficient method of analysis could be used to develop stochastic fracture models to study size effects in quasibrittle materials. For a material whose critical energy release rate is that takes independent identically distributed values according to a prescribed distribution, the crack trajectories can be described as normal distribution, $X(y) = \mu(y) + \sigma(y)Z(y)$, and as a result of the interaction of the crack with free surfaces, it exhibits path-dependence. The model procedures presented in this paper could be generalized to the cases where the microstructural parameter r_o is spatially correlated through a statistical distribution.

Acknowledgments

This research was funded by the National Science Foundation under Grants MSS94-16752 and CMS97-13997, and by ARPA under Grant DABT 63-92-C-0032.

References

- Arwade, S. (1999). Probabilistic models for aluminum microstructure and intergranular fracture analysis. M.S. Thesis, Department of Civil and Environmental Engineering, Cornell University.
- Brandinelli, L. and Ballarini, R. (2000). Stress intensity factor approximations for two-dimensional curvilinear cracks. *Composites Science and Technology* **60**, 2557–2564.
- Chen, L. (2000) Crack propagation in a material with random toughness. M.S. Thesis, Department of Civil Engineering, Case Western Reserve University.
- Chudnovsky, A. and Gorelik, M. (1996). Tortuosity of crack path, fracture toughness and scale effect in brittle fracture. In: *Size-Scale Effects in the Failure Mechanisms of Materials and Structures*. (Edited by A. Carpinteri), E&FN Spon, London, 97–108.
- Chudnovsky, A., Kunin, B. and Gorelik, M. (1997). Modeling of brittle fracture based on the concept of crack trajectory ensemble. *Engineering Fracture Mechanics* **58**(5–6), 437–457.
- Cotterell, B. and Rice, J.R. (1980). Slightly curved or kinked cracks. *International Journal of Fracture* **16**, 155–169.
- Erdogan, F., Gupta, G.D. and Cook, T.S. (1973). Numerical solution of singular integral equations. In: *Mechanics of Fracture* (edited by G.C. Sih), Vol. 1, Noordhoff, Leiden, 368–425.
- Kunin, B.I. (1994). A stochastic model for controlled discontinuous crack growth in brittle materials. In: *Probabilities and Materials* (edited by D. Breysse), Kluwer Academic Publishers, Dordrecht, 339–360.
- Kunin, B.I. and Dearth, R.S. (1998). Evaluation of statistical fracture toughness parameters on the basis of crack arrest experiment. *Prob. Engng. Mech.* **13**(3), 139–146.
- Rubinstein (1990). Crack-path effect on material toughness. *J. Appl. Mech.* **57**, 97–103.